

Article

Statistical Optimization by the Response Surface Methodology of Direct Recycled Aluminum-Alumina Metal Matrix Composite (MMC- Al_R) Employing the Metal Forming Process

Azlan Ahmad ^{1,*} , Mohd Amri Lajis ², Nur Kamilah Yusuf ² and Syaiful Nizam Ab Rahim ³¹ Department of Mechanical Engineering, Universiti Teknologi PETRONAS (UTP), Seri Iskandar 32610, Malaysia² Sustainable Manufacturing and Recycling Technology, Advanced Manufacturing and Materials Centre (SMART-AMMC), Universiti Tun Hussein Onn Malaysia (UTHM), Parit Raja 86400, Malaysia; amri@uthm.edu.my (M.A.L.); nurkamilah@uthm.edu.my (N.K.Y.)³ Department of Mechanical Engineering, Politeknik Sultan Abdul Halim Mu'adzam Shah (POLIMAS), Jitra 06000, Malaysia; syaifuln@polimas.edu.my

* Correspondence: azlan.ahmad@utp.edu.my; Tel.: +60-5368-7210

Received: 11 May 2020; Accepted: 25 June 2020; Published: 9 July 2020



Abstract: In this study, the response surface methodology (RSM) and desirability function (DF) were utilized to optimize the recycling conditions of aluminum (AA6061) chips, in the presence of particulate alumina (Al_2O_3), to obtain a metal matrix composite of recycled aluminum (MMC- Al_R) using hot press forging processes. The effects of temperature (430–530 °C) and holding time (60–120 min) were investigated. The introduction of 2.0 wt. % of Al_2O_3 to the aluminum matrix was based on preliminary research and some pilot tests. This study employed the 2^k factorial design of experiments that should satisfy the operating temperatures (T) of 430 °C and 530 °C with holding times (t) of 60 min and 120 min. The central composite design (CCD) was utilized for RSM with the axial and center point to evaluate the responses to the ultimate tensile strength (UTS), elongation to failure (ETF), and microhardness (MH). Based on RSM, with the desirability of 97.6%, the significant parameters $T = 530$ °C and $t = 120$ min were suggested to yield an optimized composite performance with UTS = 317.99 MPa, ETF = 20.45%, and MH = 86.656 HV. Three confirmation runs were performed based on the suggested optimum parameters, and the error revealed was less than 25%. The mathematical models suggested by RSM could adequately describe the MMC- Al_R responses of the factors being investigated.

Keywords: sustainable manufacturing; direct metal recycling; hot press forging; aluminum AA6061; reinforced particles; metal matrix composite

1. Introduction

Aluminum finds broad use in air, road, and sea transport, food and medicine, packaging, construction, and electronics and electrical power transmission. The production of aluminum from ores requires considerable inputs of energy [1]. Aluminum foundries contribute to 1% of the world's total manmade greenhouse emissions [2]. This negative contribution to energy consumption and the pollution caused to produce primary aluminum have made aluminum recycling, which is more economical and efficient, even more significant. Considering the high responsibility toward the environment, secondary aluminum production through a solid-state approach is a much more preferable process. In this approach, the aluminum is recycled without remelting the scrap, for the purposes of improving the recycling efficiency, energy use, and expense.

Although secondary aluminum shows good mechanical properties [3], it is generally deemed to be inferior to primary aluminum. As such, ceramic material has been introduced to improve the mechanical properties of alloys. This combination of ceramic material and metal alloys is known as a metal matrix composite (MMC). Similar to all other composites, MMCs entail at least two physically and chemically distinct phases: matrix material and reinforcing constituents. The combination of a ductile material (matrix alloys) with a high strength material (reinforcing constituent) leads to a greater strength in shear and compression and higher service temperature capabilities [4–7]. The reinforcement material for MMC can be produced in the form of continuous fibers, short fibers, whisker, or particles. Different from unreinforced compounds, all fortification structures have the possibility to introduce fundamentally better preservation of the anisotropic properties and explicit properties at room temperature and high temperatures [8–11].

As the awareness of the importance of MMCs grows, many interested parties have taken the initiative to continue developing the proper techniques for MMC fabrication. There are several methods currently being practiced both by industry and researchers. Generally, MMC fabrication can be classified into three categories: (a) liquid-state processing, (b) solid-state processing, and (c) gaseous processing. Figure 1 elaborates these three categories in a well-structured diagram.

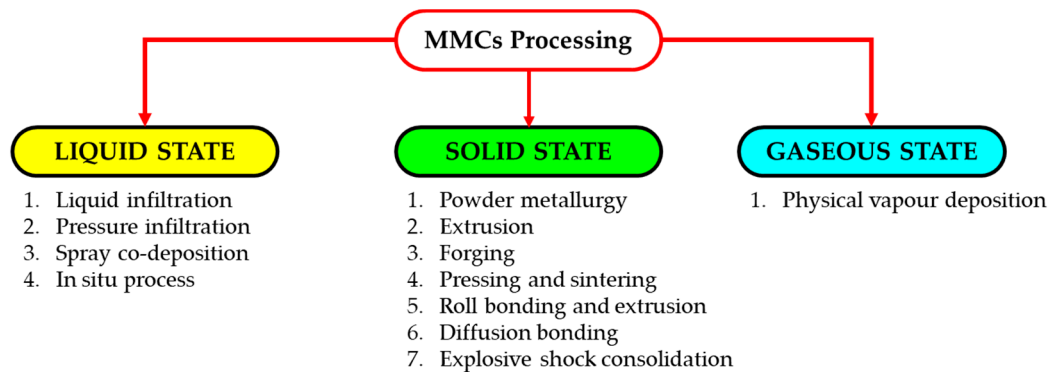


Figure 1. Metal matrix composite processing categories.

Forging transforms a simple part geometry into a complex one, whereby the tools take the shape of the desired geometry and impart pressure on the deforming material through the tool interface [12]. Among all metal forming techniques, forging has an extraordinary place since it tends to be utilized to deliver some of the predominant mechanical properties with the least waste of the material [13,14]. Room temperature forging is commonly known as cold forging. However, if the temperature is above the material recrystallization temperature, it is classified as hot forging. The approach of direct recycling of aluminum, using hot press forging, eliminates two pre-processing steps, which are cold compaction and ball-milling, thus reducing the time, cost, and energy consumption [15]. Previous studies discussed the contribution of the operating temperature to the increase in the strength of materials [16–20]. In addition, by employing the response surface methodology (RSM) in the experimental study, the quadratic effects of multiple responses can be optimized to fit an ideal parameter selection. Lajis et al. (2014) obtained an adequate equation to best fit the ultimate tensile strength (UTS) response when varying the chip size, temperature, and pressure [18]. Likewise, Khamis et al. (2014) employed full factorial central composite design (CCD) by varying the aluminum chip size, pre-compacting cycle, and holding time. Consequently, the results of an ANOVA test suggested 98% desirability with a reasonable $Pred R^2$ of 89%, making time the vital factor for increasing the UTS, compared to the other factors [21].

Notwithstanding the different breakthroughs made throughout the years with respect to MMC manufacture, there are restricted applications that require advanced methods. This is because of the problems experienced in shaping the final product appropriately, where the machining procedure could cause surface damage, possibly impacting some desirable properties: fatigue and corrosion

resistance [22]. Thus, it is beneficial to utilize the hot press forging process, to achieve a close net-shaped product, without causing such damage. Besides, such a plastic deformation approach offers the possibility of improving the anisotropic properties by solidifying the grid and adjusting the microstructural properties, for example the porosity [4,22,23].

To the authors' knowledge, there are no studies concerning producing MMCs by using machining scraps. Realizing the huge potential of the hot press forging process, therefore, it is crucial to employ such a technique in producing MMCs without altering the initial form of the scrap. In the present work, the goal is to employ the full-factorial central composite design as a DOE method to conduct the modelling process and investigate the effect of parameters such as the operating temperature and holding time on the tensile strength, elongation, and hardness of MMC- Al_R . The novelty of the direct conversion of aluminum chips reinforced with Al_2O_3 particles is the ultimate contribution of this study.

2. Methodology

2.1. Material

As-cast aluminum 6061 bulk series and alumina (Al_2O_3) powder sized $\sim 1 \mu m$ with 99.9% purity were obtained from commercial vendors. Al_2O_3 was chosen as the reinforcement material due to it being chemically inert with aluminum, while it can also be used at a higher temperature, compared to unreinforced aluminum [24]. In addition, particles or discontinuously reinforced constituents provide many benefits for composites, including high modulus and strength, improved thermal stability, better wear resistance, and relatively better isotropic properties, compared to fiber reinforced composites [4]. The material investigated in this study was milled from pure as-cast AA6061 bulk. The bulk was inspected and confirmed to comply with the Standard Specification for Aluminium and Aluminium-Alloy Sheet and Plate (ASTM B209). The 6xxx series aluminum consists of Al-Mg-Si, and all of these elements appeared in the test specimen. The composition was balanced with respect to the content of Si, Mg, and Al. By referring to Figure 2, aluminum showed the highest peak of the elements, and the others were Mg (5.84 wt. %), Si (0.17 wt. %), and other elements (<0.01 wt. %) [23]. The composition of 99.9 % purity Al_2O_3 (Sigma-Aldrich, Saint Louis, MO, USA) with a size of $\sim 1 \mu m$ mainly consisted of aluminum (Al) and oxide (O).

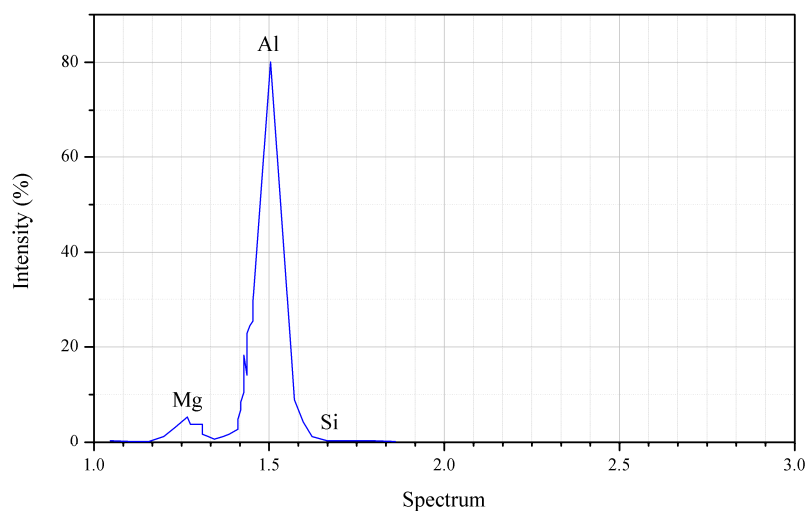


Figure 2. EDS spectra for AA6061 [23].

2.2. Preparation

AA6061 bulk was milled using Sodick-MC430L high-speed machining (Baginton, Coventry, UK), and chips were produced by manipulating the machining parameters. It was revealed that a medium

chip size (length 5.20 mm, width 1.097 mm, thickness 0.091 mm) yielded better specimen performance, and the machining parameters are presented in Table 1 [15,25–27].

Table 1. Selected milling parameters.

Parameters	Cutting Speed, v (m/min)	Feed, f (mm/tooth)	Depth of Cut (DOC) (mm)
Value	1100	0.05	1.0

Cleaning of the produced chips was done using 99.5% purity acetone (C_3H_6O) right after the milling process before the drying process in a thermal oven at 60 °C, which took about 30 min. The Al_2O_3 powder of 2.0 wt % was loaded into the mixing chamber, with the aluminum chips making up the remaining 98 wt % of the total composite weight. Cleaned aluminum chips were mixed with Al_2O_3 powder in the SYL 3 Dimensional Mixer at a speed of 50 rpm. Previously, it was reported that any excessive addition of reinforcing particles to the recycled aluminum could jeopardize the composite's performance [28]. It was suggested that only 2.0 wt % of Al_2O_3 was sufficient for the composite.

2.3. Experimental Procedure

A total of 12.0 g of clean and dry aluminum chips were poured into the mold, and the plunger was fixed accordingly [15,29]. Subsequently, the mold was placed inside the hot press forging machine for the forming operation. For the hot forging process of AA6061, the selected operating temperature and force were 530 °C and 350 kN, respectively. Referring to Figure 3, the mold was heated until the desired temperature was achieved and maintained for 30 min to allow for a uniform heat distribution within the mold and the test composite it contained, and during the period of the pre-compacting cycle (PCC), the plunger was repeatedly pressed with the desired force for several cycles, as depicted in Figure 3c. The temperature and force were maintained until the end of the soaking time. Finally, the temperature controller was turned off to begin the cooling stage, while the plunger was left stationary (at the maximum force). The material come out following the dog bone standard test shape with the dimension of 100 mm × 5 mm × 10 mm.

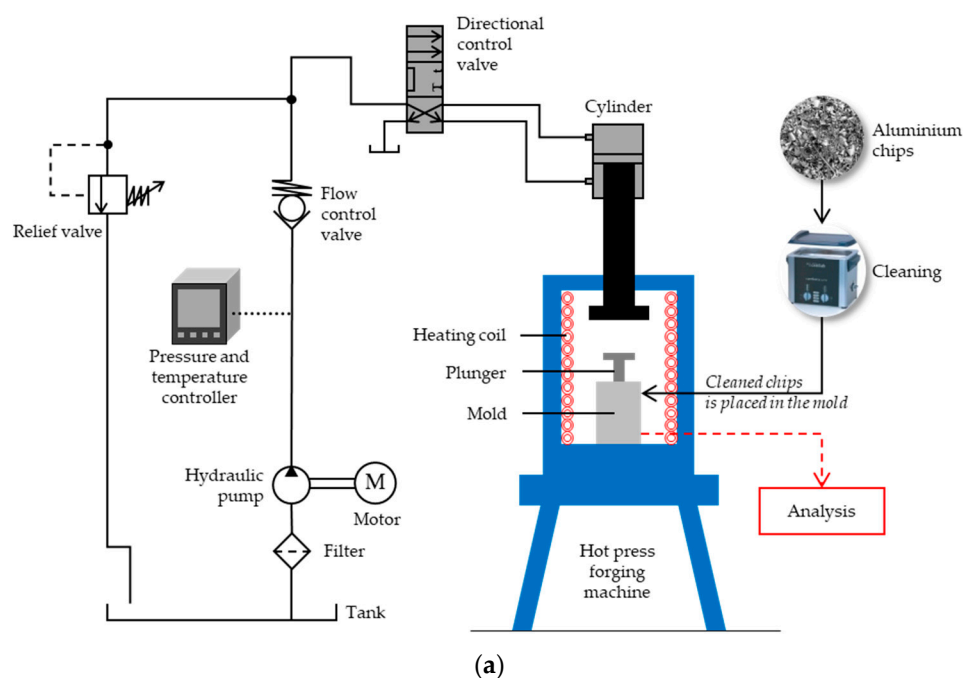


Figure 3. Cont.

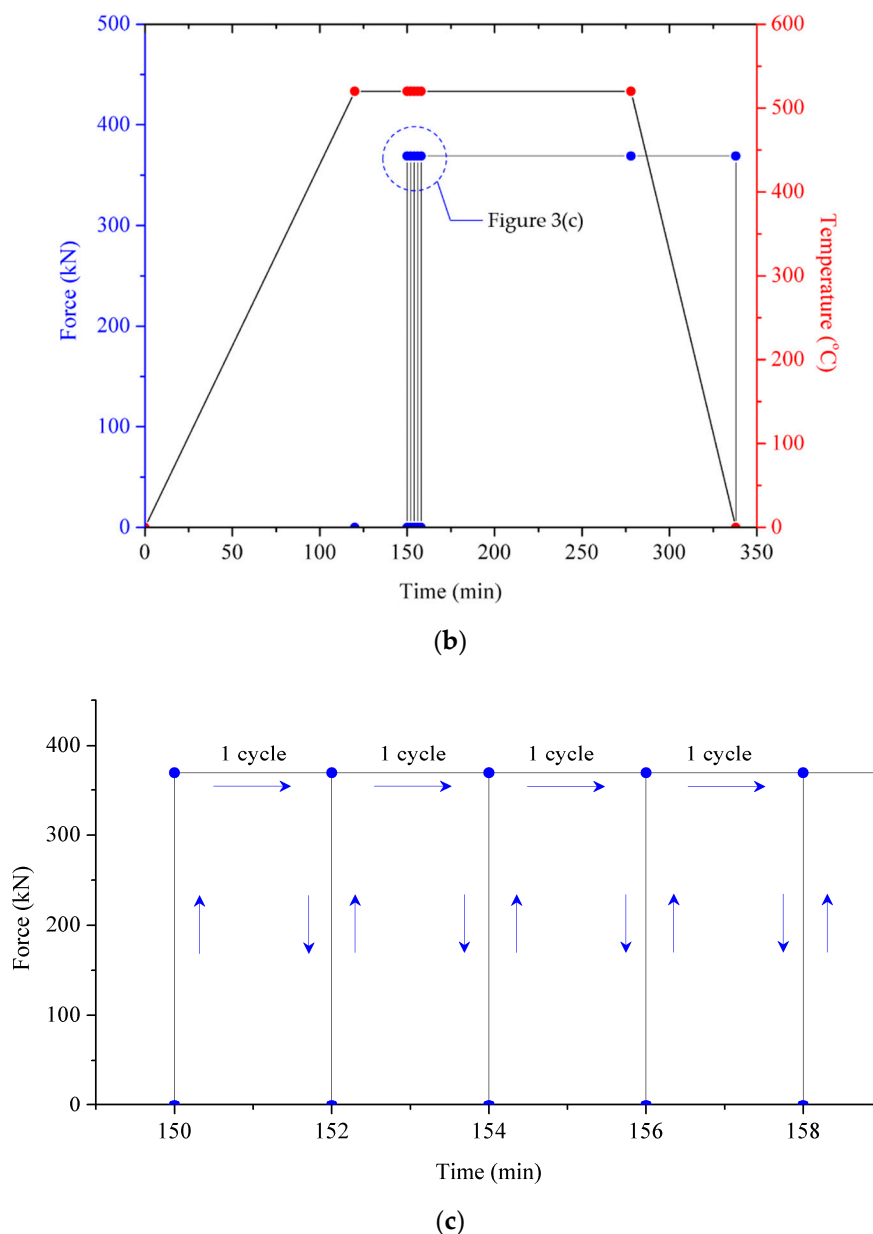


Figure 3. Hot press forging (a) overall process, (b) force-temperature parameter, and (c) time interval during the forging phase [23].

2.4. Response Surface Methodology

The common practice to evaluate the material integrity is done by studying one factor at a time. Such a practice was unable to evaluate the material since the study did not include the interactions amongst the factors. Either the interaction effect was significant or not; yet, each of the factors contributed to the material integrity [30]. Along these lines, it was pivotal to utilize the design of experiments (DOE) in the investigation since it helped in estimating the connections between the elements with the imperative factors [31]. In addition, the response surface methodology (RSM) is a useful tool for developing, improving, and optimizing processes by statistical and mathematical techniques [32]. By utilizing RSM, it additionally could decrease the quantity of experimental preliminaries and assess the connections between different parameters. These favorable circumstances make RSM less arduous and tedious than the other advanced strategies such as the Taguchi method [33].

In this study, RSM was utilized to survey the connection between the three reactions (UTS, elongation to failure (ETF), and microhardness (MH)) and the two most significant parameters

(temperature and holding time), so as to simplify the important states of the parameters to anticipate the best reactions. The experiments were improved with replications at the design center to evaluate the pure error and were done in a randomized order, as required in many design methods. A coded design variable was utilized in this examination, as it was dimensionless and could quantify the impact of changing each design factor over a one-unit interval. Coded designs can be straightforwardly contrasted with the extent of the model coefficients, and the relationship is bounded as in Equation (1) [34].

$$C = \frac{X - \frac{(A_l + A_h)}{2}}{\frac{(A_h - A_l)}{2}} \quad (1)$$

where C is the coded design variable; X is the actual intended magnitude; A_l and A_h are the actual low and high magnitudes, respectively. Since there are only three levels for each factor, the proper model for predicting the ideal conditions is in the accompanying quadratic model structure as in Equation (2) [35].

$$y = \beta_0 + \sum_{j=1}^k \beta_j x_j + \sum_{j=1}^k \beta_{jj} x_j^2 + \sum_i \sum_{<j=2}^k \beta_{ij} x_i x_j + \epsilon_i \quad (2)$$

where y is the response; x_i and x_j are the factors; β_0 is a constant coefficient; β_j , β_{jj} , and β_{ij} are the interaction coefficients of the linear, quadratic, and second-order terms, respectively; k is the number of studied factors; and ϵ_i is the error. The fit polynomial equation is expressed as surface and contour plots in order to visualize the relationships between the response and experimental levels of each factor and to deduce the optimum conditions [36,37]. After optimization, the sufficiency of the model conditions for predicting the ideal reaction conditions was validated with the experimental outcomes.

The desirability function is a target that ranges from zero outside of the cut-off points to one at the objective. The qualities of an objective might be changed by altering the weight or significance. For a few reactions and elements, all objectives must be advanced at the same time as one desirability function. Equation (3) depicts the combined objective function, which is the geometric mean of all transformed responses.

$$D = (d_1 \times d_2 \times \dots \times d_n)^{\frac{1}{n}} = \left[\prod_{i=1}^n d_i \right]^{\frac{1}{n}} \quad (3)$$

where D is the overall desirability and n is the number of responses in the measure. If any of the reactions or elements fall outside the desirability range, the general function becomes zero. For synchronous optimization, every reaction must have a low and a high value given to every objective. Derringer and Suich proposed different desirability functions d , depending on whether a particular response y is to be minimized, maximized, or assigned a target value [34,38,39]. This study involved determining a single set of process conditions, maximizing the three responses (UTS, ETF, and MH) simultaneously. Figure 4 depicts the desirability function for maximizing response y , where y is the response value, L and T are the lower limit and target of the response, respectively, and w is the weight coefficient, with the weight being maintained at a value of one (1) so as not to be affected by different output variables [40].

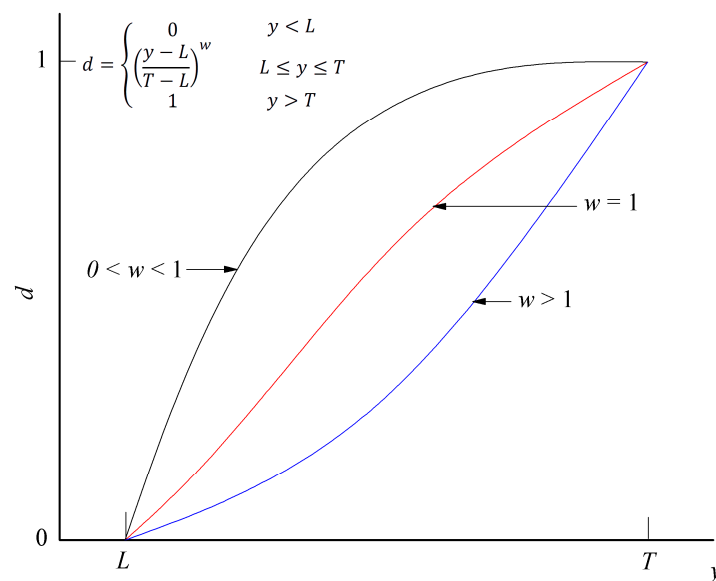


Figure 4. Desirability function targeted to maximize y .

2.5. Experimental Design

The forging process employed the central composite design (CCD), which is the factorial portion of a full factorial design, with all combinations of the factors being at two levels. The star points were located at the face of the cube portion of the design. The points corresponded to an α -value of 1 (face-centered). The center points were points with all levels set to Coded Level 0, at the midpoint of each factor's range and repeated twice. In this particular investigation, two factors were studied, and their low and high levels (using Equation (1)) are given in Table 2. The forging process was carried out on a hot press forging machine at a constant axial force of 35 ton.

Table 2. Factors and levels for the response surface study.

Factors	Unit	Notation	Levels		
			(−1)	(0)	(+1)
Temperature	°C	x_1	430	480	530
Holding time	min	x_2	60	90	120

The response variables investigated were the ultimate tensile strength (y_1), elongation to failure (y_2), and MH (y_3). Based on the foregoing input to the completed design layout produced by the software, the actual midpoint values to be used were reflected, i.e., 480 °C for temperature and 90 min for holding time.

2.6. Experimental Techniques

There were a total of 11 trials conducted, which involved 3 responses for each run. The measured responses were UTS, ETF, and MH. The UTS and ETF tests were performed by using the ultimate tensile machine GOTECH AI-7000 (Taichung, Taiwan) at room temperature with a test speed of 0.50mm/min. For the MH responses, the test was performed using a Vickers hardness tester Shimadzu HMV-2TE (Tokyo, Japan) by forcing (2.942 N) a square-based pyramidal diamond indenter having face angles of 136°. The time of application of the full test was 10 s, involving 10 randomly distributed indentations for each run. The density was measured by using a density balance, conducted following the Archimedean method [41]. The microstructures of the composite were examined under an optical microscope Olympus BX60M (Tokyo, Japan).

3. Results and Analysis

The results of the forging operation performed as per the experimental plan are shown in Table 3. The array was calculated using Equation (1), and the actual values were practically chosen from the low and high ends of the parameter range. These results were used as the input for further analysis by the Design Expert 8.0 software (Minneapolis, MN, US). Without performing any modification on the response, each source term was examined for the probability (“Prob > F”). The “lack of fit tests” table compares residual error with “pure error” from replicated design points. The desired model should have a “Prob > F” value above 0.05. The quadratic model, identified as the likely model, was selected, as it did not show a significant lack of fit, and it turned out to be the best in the “model summary statistics”. It exhibited low standard deviations (“Std. Dev.”), high “R-squared” values, and a low “PRESS”. The program automatically underlined at least one “suggested” model. In short, the examination of the fit summary for all responses revealed the quadratic model to be statistically significant, and therefore, it was used for further analysis.

Table 3. Completed design layout.

Std. Run	Factors (Coded)		Factors (Actual)		Experiment		
	C ₁	C ₂	x ₁ (°C)	x ₂ (min)	y ₁ (MPa)	y ₂ (%)	y ₃ (HV)
1	−1	−1	430	60	19.20	2.07	71.360
2	+1	−1	530	60	273.94	13.99	80.592
3	−1	+1	430	120	27.82	2.24	74.625
4	+1	+1	530	120	317.99	20.45	86.656
5	−1	0	430	90	22.31	2.22	73.367
6	+1	0	530	90	297.10	17.90	83.921
7	0	−1	480	60	169.20	4.17	76.432
8	0	+1	480	120	188.11	6.69	78.454
9	0	0	480	90	175.76	5.90	76.662
10	0	0	480	90	180.49	5.52	76.503
11	0	0	480	90	170.71	4.88	76.988

3.1. Analysis of Variance of the Properties Affected by the Process Parameters

The ANOVA table for the response surface of a quadratic model for all responses is shown in Table 4. The model F-value of 1548.26, 446.42, and 62.49 for UTS, ETF and MH, respectively, suggested that the model was significant since there was only a 0.01%–0.02% chance that a “model F-value” this large could occur due to noise. Values of “Prob > F” less than 0.05 showed that the model terms were significant and desirable as they indicated that the terms in the model had a significant effect on the responses [33]. Corresponding to that, the main effect of temperature (x_1), holding time (x_2), the two level interaction of temperature and holding time (x_1x_2), and the second-order effect of temperature (x_1^2) were significant model terms for UTS and ETF. However, for MH, only x_1 , x_2 , and x_1^2 were significant model terms. On the contrary, the other model terms were not significant as the “Prob > F” values were greater than 0.05. These insignificant model terms could be removed, and an improved model could be produced as a result. The “lack of fit F-value” of 0.36, 0.53, and 16.58 for UTS, ETF, and MH, respectively, implied that there was a 79.29%, 70.51%, and 5.74% chance that a “lack of fit F-value” this large could occur due to noise. All models were considered to be adequate since this was not significant in the lack of fit test.

Table 4. ANOVA table (partial sum of squares) for the initial quadratic model. UTS, ultimate tensile strength; Adeq., adequate; ETF, elongation to failure; MH, microhardness.

Source	Sum of Squares	df	Mean Square	F-Value	Prob > F
UTS (MPa)					
Model	113,957.73	5	22,791.55	1548.26	<0.0001 ^s
x_1	111,984.68	1	111,984.68	7607.29	<0.0001 ^s
x_2	853.95	1	853.95	58.01	0.0006 ^s
$x_1 x_2$	313.82	1	313.82	21.32	0.0058 ^s
x_1^2	776.81	1	776.81	52.77	0.0008 ^s
x_2^2	5.25	1	5.25	0.36	0.5766 ^{ns}
Residual	73.60	5	14.72		
Lack of Fit	25.76	3	8.59	0.36	0.7929 ^{ns}
Pure Error	47.84	2	23.92		
R ² = 0.9994, R ² _{adj} = 0.9987, R ² _{pred} = 0.9970, Adeq. precision = 104.845					
ETF (%)					
Model	426.02	5	85.20	446.42	<0.0001 ^s
x_1	349.76	1	349.76	1832.56	<0.0001 ^s
x_2	13.95	1	13.95	73.11	0.0004 ^s
$x_1 x_2$	9.89	1	9.89	51.82	0.0008 ^s
x_1^2	49.77	1	49.77	260.77	<0.0001 ^s
x_2^2	0.099	1	0.099	0.52	0.5038 ^{ns}
Residual	0.95	5	0.19		
Lack of Fit	0.42	3	0.14	0.53	0.7051 ^{ns}
Pure Error	0.53	2	0.27		
R ² = 0.9978, R ² _{adj} = 0.9955, R ² _{pred} = 0.9880, Adeq. precision = 57.074					
MH (HV)					
Model	197.66	5	39.53	62.49	0.0002 ^s
x_1	168.72	1	168.72	266.71	<0.0001 ^s
x_2	21.47	1	21.47	33.95	0.0021 ^s
$x_1 x_2$	1.96	1	1.96	3.10	0.1388 ^{ns}
x_1^2	4.74	1	4.74	7.49	0.0409 ^s
x_2^2	0.071	1	0.071	0.11	0.7520 ^{ns}
Residual	3.16	5	0.63		
Lack of Fit	3.04	3	1.01	16.58	0.0574 ^{ns}
Pure Error	0.12	2	0.061		
R ² = 0.9843, R ² _{adj} = 0.9685, R ² _{pred} = 0.8520, Adeq. precision = 24.496					

^s Significant at $p < 0.05$; ^{ns} not significant at $p > 0.05$.

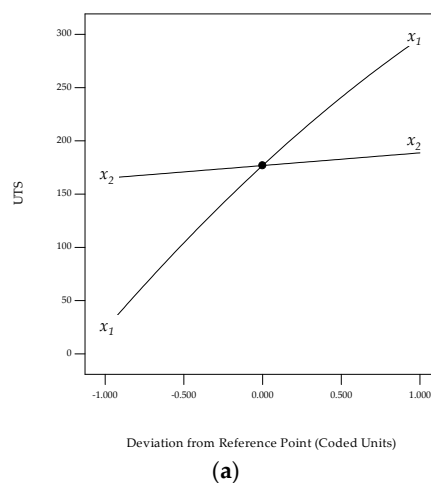
It was apparent that there were terms that might be eliminated to increase the accuracy of the model. The non-significant terms were automatically reduced by a backward elimination process, and the resulting ANOVA table for the reduced quadratic model for all responses is shown in Table 5. It can be noticed that the models were still significant, and the lack of fit remained non-significant. However, some of the factors were eliminated from the model. The main effect of x_1 was found to be the most significant factor associated with all responses. Additionally, the determination coefficient, R^2 , should be at least 0.80 for a good model fit [42]. Prior to that statement, the R^2 value reduction from the previous model, indicating only 0.07%, 0.25% and 2.59% of the total variation for UTS, ETF, and MH, respectively, was not explained by the model. The " R^2_{pred} " close to one was in a reasonable agreement with the " R^2_{adj} ". The high value of the adjusted R^2 indicated the strong significance of the model [43]. Adequate precision is the signal-to-noise ratio, which compares the range of the predicted values at the design points to the average prediction error. Ratios greater than four indicate adequate model discrimination. Since the ratio for all responses indicated an adequate signal, this model could be used to navigate the design space.

Table 5. ANOVA table (partial sum of squares) for the reduced quadratic model.

Source	Sum of Squares	df	Mean Square	F-Value	Prob > F
UTS (MPa)					
Model	113,952.49	4	28,488.12	2167.80	<0.0001 ^s
x_1	111,984.68	1	111,984.68	8521.46	<0.0001 ^s
x_2	853.95	1	853.95	64.98	0.0002 ^s
$x_1 x_2$	313.82	1	313.82	23.88	0.0027 ^s
x_1^2	800.03	1	800.03	60.88	0.0002 ^s
Residual	78.85	6	13.14		
Lack of Fit	31.01	4	7.75	0.32	0.8454 ^{ns}
Pure Error	47.84	2	23.92		
R ² = 0.9993, R ² _{adj} = 0.9988, R ² _{pred} = 0.9979, Adeq. Precision = 121.558					
ETF (%)					
Model	425.92	4	106.48	606.58	<0.0001 ^s
x_1	349.76	1	349.76	1992.48	<0.0001 ^s
x_2	13.95	1	13.95	79.49	0.0001 ^s
$x_1 x_2$	9.89	1	9.89	56.35	0.0003 ^s
x_1^2	52.31	1	52.31	298.01	<0.0001 ^s
Residual	1.05	6	0.18		
Lack of Fit	0.52	4	0.13	0.49	0.7546 ^{ns}
Pure Error	0.53	2	0.27		
R ² = 0.9975, R ² _{adj} = 0.9959, R ² _{pred} = 0.9896, Adeq. Precision = 65.192					
MH (HV)					
Model	195.63	3	65.21	87.92	<0.0001 ^s
x_1	168.72	1	168.72	227.47	<0.0001 ^s
x_2	21.47	1	21.47	28.95	0.0010 ^s
x_1^2	5.44	1	5.44	7.33	0.0303 ^s
Residual	5.19	7	0.74		
Lack of Fit	5.07	5	1.01	16.59	0.0578 ^{ns}
Pure Error	0.12	2	0.061		
R ² = 0.9741, R ² _{adj} = 0.9631, R ² _{pred} = 0.9165, Adeq. Precision = 27.707					

^s Significant at $p < 0.05$; ^{ns} not significant at $p > 0.05$.

The adequacy of the model can also be assessed using the perturbation plot and surface graphic. Figure 5 shows the perturbation plot for UTS, ETF, and MH, which indicated that the main effect of temperature had more influence on the main effect of holding time in order to have a better UTS response. Figure 6 depicts the 3D surface graphic with respect to the main effects of temperature and holding time. As can be noticed, an increase in the holding time and temperature caused a corresponding increase in the composite performances.

**Figure 5.** Cont.

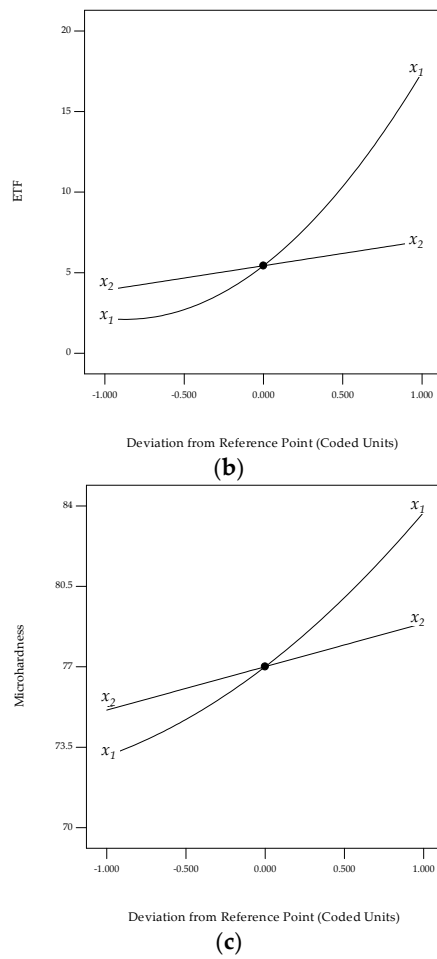


Figure 5. Perturbation plot of the factors for (a) UTS, (b) ETF, and (c) MH.

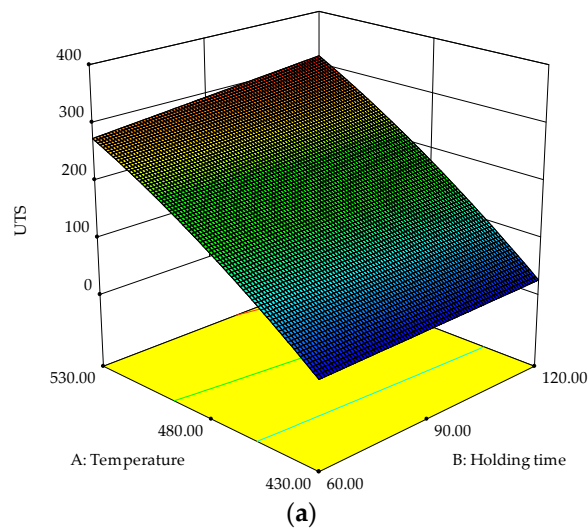


Figure 6. Cont.

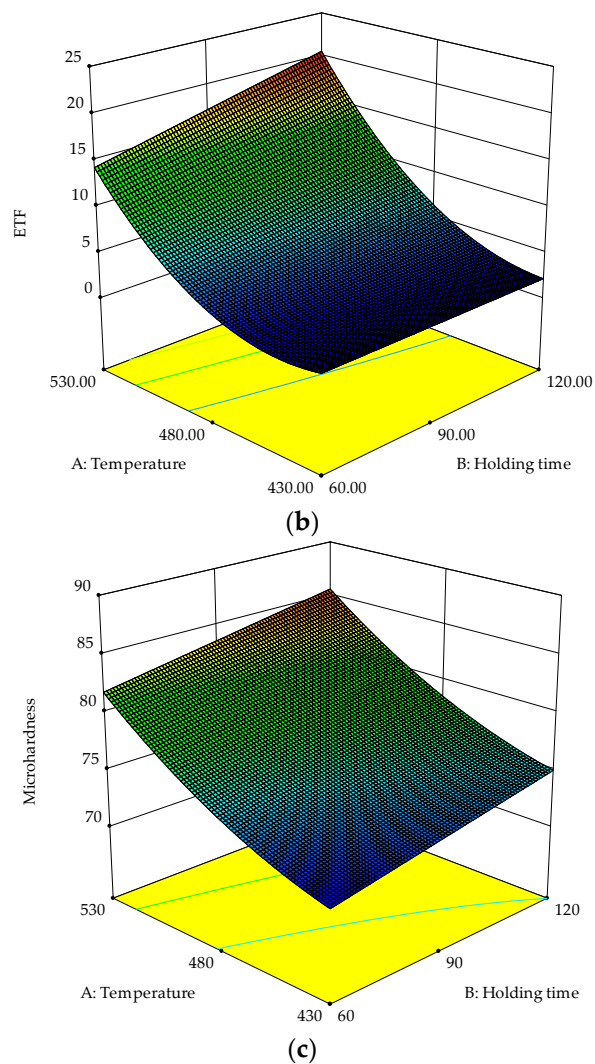


Figure 6. 3D surface graphic of the factors for (a) UTS, (b) ETF, and (c) MH.

3.2. Empirical Relationship of the Independent Variables

RSM gives the predicted models as far as coded and actual variables are concerned. Coding makes a direct representation between coefficients conceivable, while the actual terms change contingent upon the unit of measure. These terms could be utilized to represent the consequences of this study; however, they cannot be utilized for displaying future reactions. The program prescribed the utilization of the quadratic model structure for every single factor variable. Subsequent to removing the non-critical terms, the last experimental relationship (as far as the coded factors are concerned) for all reactions can be expressed as Equations (4)–(6):

$$UTS = 176.85 + 136.62 (T) + 11.93 (HT) + 8.86 (T)(HT) - 17.13 (T^2) \quad (4)$$

$$ETF = + 5.43 + 7.64 (T) + 1.53 (HT) + 1.57 x_1 x_2 + 4.38 (T^2) \quad (5)$$

$$MH = + 77.01 + 5.30 (T) + 1.89 (HT) + 1.41 (T^2) \quad (6)$$

These models were shown to be an adequate representation of the response (UTS, ETF, and MH). By comparing Equations (4)–(6) with Equation (2) in Section 2.4, one can notice that $\beta_1 > \beta_2$ for all the responses. It could be concluded that the factor A (temperature) had the greatest effect on all responses due to its coefficient being the highest. Throughout the prediction models above, there were factors that interacted with each other, indicating either the synergistic or antagonistic effects of two

factors. The positive β_{12} values obtained for both UTS (+8.86) and ETF (+1.57) showed the synergistic effects experienced, meaning that a combination of the factors *A* and *B* (temperature and holding time) produced higher value responses than would be expected just by single factor effects. On the contrary, β_{11} appeared to have positive and negative coefficients, which indicated that it experienced both synergistic effects for ETF (+4.38) and MH (+1.41), as well as antagonistic effects for UTS (−17.13). The second-order effect of temperature would lower the UTS, while increasing the ETF and MH of the composite.

3.3. Process Optimization and Confirmation Runs

Earlier, the investigations depended on the individual outcome of UTS, ETF, and MH. In this study, the goal was to get the feasible region of optimization through the overlaying contour plots. This strategy included individual overlaying of all responses' contour plots and finding the zone that was the most ideal for every one of the responses. Figure 7 delineates the overlay contour plots for UTS, ETF, and MH. The grey area on the plot does not meet the desirability, while the lines denote the high or low limits on the responses. The region in yellow demonstrates the practical area to set the variables to fulfil the desirability. The objective of this study was to determine the optimum parameters that should be chosen to produce a great mechanical performance of the composite. In order to do so, all responses should have a maximum value. Table 6 shows the anticipated parameters recommended by RSM to acquire ideal responses. The results of the experiments showed that the suggested temperature of 530 °C and holding time of 120 min gave the highest desirability of 97.6%, yielding the UTS, ETF, and MH of 317.61 MPa, 20.54%, and 85.615 HV, respectively.

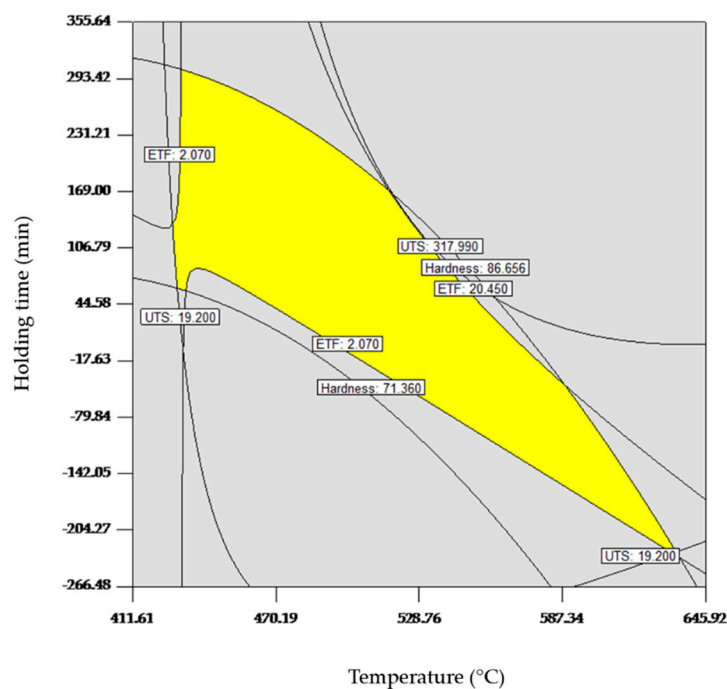


Figure 7. Overlay plot for optimization.

Table 6. Suggested solution for optimum responses.

Solutions	Temperature (°C)	Holding Time (min)	UTS (MPa)	ETF (%)	MH (HV)	Desirability
1	530.00	120.00	317.61	20.54	85.615	0.976 *
2	529.48	120.00	316.46	20.36	85.531	0.972
3	527.44	120.00	311.91	19.64	85.202	0.946
4	530.00	109.12	309.22	19.42	84.929	0.933
5	530.00	86.71	293.12	17.11	83.516	0.842

* Selected since the desirability is highest compared to other solutions.

To verify the sufficiency of the generated model, three verification run tests were performed. The reaction conditions inferred before were utilized as the expectation for the actual value. Table 7 records the qualities of the verification runs and the correlation made against the anticipated designed for UTS, ETF, and MH. The test condition for the first run was the ideal recommended condition, while the other two runs were not, however still within the range as previously shown in the table.

Table 7. Confirmation experiments.

Responses	Factors	Run		
		1	2	3
	Temperature (°C)	530	500	450
	Holding Time (min)	120	70	100
UTS	Actual	330.69	218.82	108.76
	Predicted	317.13	218.45	90.92
	Error (%)	4.10	0.17	16.40
ETF	Actual	23.09	8.78	2.11
	Predicted	20.55	7.75	2.62
	Error (%)	11.00	11.73	24.17
MH	Actual	84.18	78.53	74.11
	Predicted	85.62	78.09	74.97
	Error (%)	1.71	0.56	1.16

Throughout the analysis, it was revealed that the error recorded was acceptable. The maximum errors obtained for UTS, ETF, and MH were 16.40%, 24.17%, and 1.71% respectively. Evidently, the small error obtained from the confirmation runs supported the statistical validity of the model. Figure 8 below depicts the responses for UTS, ETF, and MH for each confirmation run, corresponding to the predicted and actual values. Clearly, the residuals between both the predicted and actual values were hardly noticeable. In short, the models developed were reasonably accurate for all responses as all confirmation runs were within 95% of the predicted value. As the desired mechanical properties of forging can only be obtained by means of a final heat treatment (T5-temper), aging after the forging process was discussed by Yusuf et al. (2017). The performance of the recycled aluminum chips was compared between both untreated (T1) and heat treated (T5) chips. The T1 recycled chip was considered comparable to the theoretical AA6061 T4, while the T5 recycled billet was considered comparable to the as-received AA6061 T6, where the value of the microhardness at 175 °C and 120 min of aging was revealed to be greater than 3.18% [14].

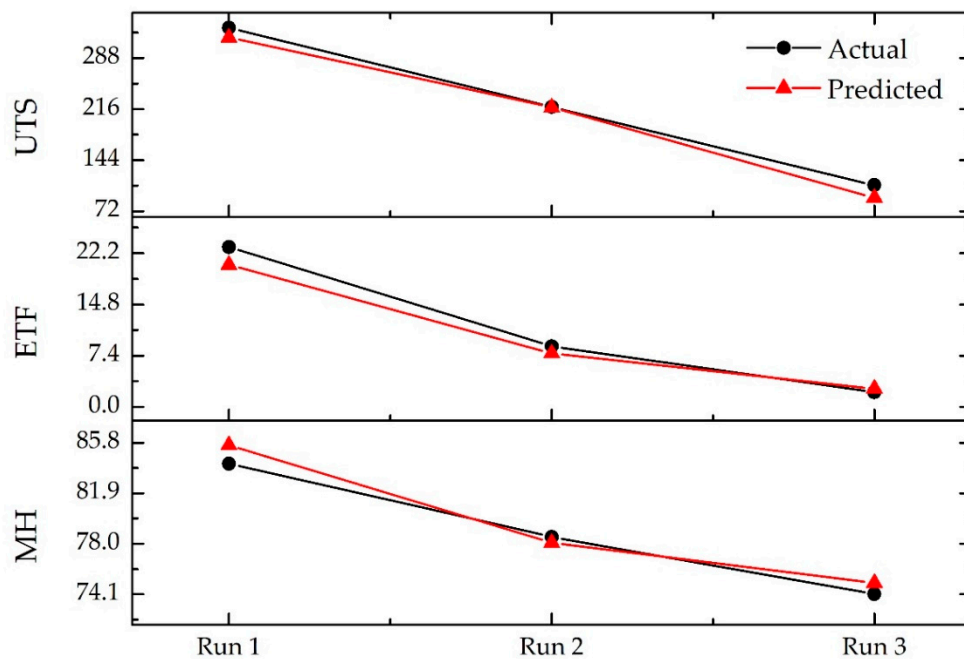


Figure 8. Errors between actual and predicted values in the confirmation runs for UTS, ETF, and MH.

3.4. Density Analysis

The influence of temperature at various holding times on the density of the composites is shown in Figure 9. As is clear, the density of the composites improved as the holding time and the temperature increased. Deficient temperature and holding time caused the composite to have substantial voids, resulting in a low density. When exposing composites to a higher temperature, the voids became smaller, and the micro-sized Al_2O_3 was able to occupy the opening and directly work to strengthen the ductile aluminum. This process was facilitated by the increment of the holding time to permit the composite to have better adhesion between the chips. The proper combination of temperature and holding time would allow the composite to achieve a good density.

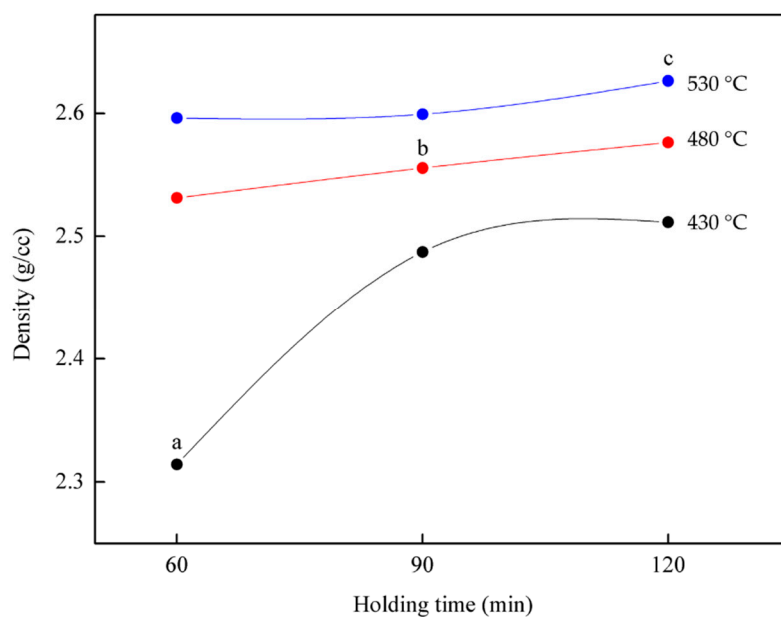


Figure 9. Density variation at different temperatures.

Moreover, a large difference in the densities of both aluminum and Al_2O_3 , which were the constituents forming the composite, was another factor for the density increment [44]. The rule of the mixtures as formulated in Equation (7) could be used to explain the relationship between both constituents mathematically [45].

$$\rho_c = (\rho_m \times f_m) + \rho_r(1 - f_m) \quad (7)$$

where ρ_c , ρ_m , and ρ_r are the theoretical densities for the composite, matrix (AA6061; 2.7 g/cm^3), and reinforcing constituent (Al_2O_3 ; 3.97 g/cm^3), respectively, and f_m the volume fraction for the matrix (98 wt %). Using Equation (7), the composite density obtained was 2.7254 g/cm^3 . By comparing the value with the experimental value, at the maximum holding time and the maximum temperature, the smallest error found was 1.53%. This directly supported the statistical validity of the model generated via RSM. Moreover, compared to the previous study by Yusuf [14], the additional presence of alumina reinforcement particles increased the composite density by 1.28%. The void-filling activities enhanced the composite density. The density enhancement experienced in this study was shown by the microstructures of the composite, as illustrated in Figure 10.

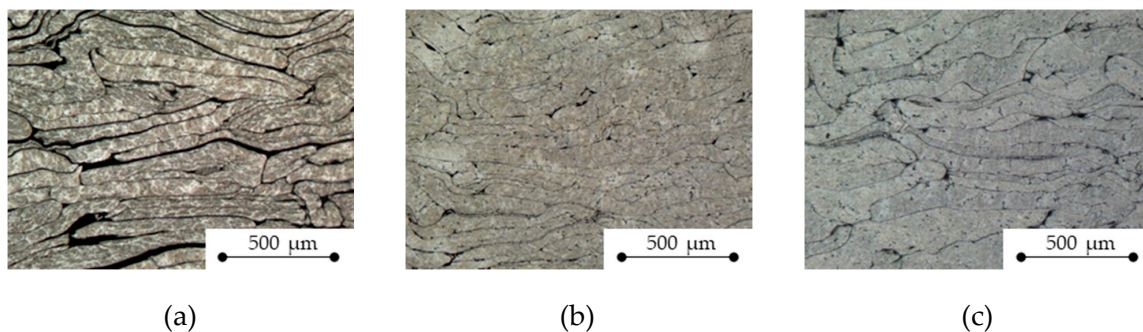


Figure 10. The optical microstructure of the composite at the parameters set as the (a) minimum, (b) intermediate, and (c) maximum.

Figure 10 shows the respective microstructures corresponding to Points a, b, and c marked in Figure 9. As can be noticed, an increase in the temperature and holding time caused a decrease in the void size between chips. This resulted in the Al_2O_3 particles more easily filling the voids and decreased the porosity, thus enhancing the density of the composite. In another study on the material integrity, it was shown that the internal strain was unintentionally altered during the hot press forging process, which may have resulted in a different degree of plastic deformation in the composite grains. Additionally, a high operating temperature and holding time contributed to the increase in the crystalline size. The Al_2O_3 also acted as a catalyst for the structural size change. Hard ceramic particles introduced into the composite caused the matrix to expand in all directions, creating better bonding in the matrix, thus yield better performance of MMC- Al_R [23]. Furthermore, the analysis of the grain structure showed that the grain average diameter reduced as the temperature and holding time increased. The grain growth of the composite was suppressed by the ceramic additive, which improved the material properties.

4. Conclusions

The effects of varying the temperature and holding time on UTS, ETF, and MH were investigated using RSM.

- The ANOVA results revealed that temperature was the most influential parameter on all responses, followed by holding time, which was found to affect the responses less significantly. The second-order effect of temperature provided a contribution to all responses, while synergistic

effects occurred due to the factor AB (temperature and holding time interaction), implying that a particular combination of parameters produced higher responses, only for UTS and ETF.

- The combination of high temperature and high holding time yielded high UTS, ETF, and MH.
- The reduced empirical models developed were reasonably accurate since the difference between the actual residual value and the predicted residual value was small. The quadratic models could be used for prediction within the limits of the factors investigated.
- The pressing action assisted by high heat was responsible for the accumulation of Al_2O_3 in the gaps between the chips by promoting relaxation of the materials. These void-filling activities reduced the porosity and hence caused a high composite density.
- The gaps between aluminum chips decreased with the increase in temperature and holding time, due to the presence of Al_2O_3 particles.

Author Contributions: All authors read and agree to the published version of the manuscript. Conceptualization, A.A.; data curation, A.A.; formal analysis, A.A.; funding acquisition, M.A.L.; investigation, A.A. and N.K.Y.; methodology, A.A. and S.N.A.R.; resources, M.A.L.; supervision, M.A.L.; validation, A.A.; writing, original draft, A.A.; writing, review and editing, A.A.

Funding: This research was funded by the Ministry of Higher Education (MOHE), Malaysia, through the Malaysian Technical University Network-Centre of Excellence (MTUN-CoE) and the Fundamental Research Grant Scheme (FRGS) Grant Numbers 1496, 1463, and 015MA0-009.

Acknowledgments: The authors want to offer their sincere thanks to the Ministry of Higher Education (MOHE), Malaysia, Sustainable Manufacturing and Recycling Technology, Advanced Manufacturing and Materials Center (SMART-AMMC), Universiti Tun Hussein Onn Malaysia (UTHM), and Universiti Teknologi PETRONAS (UTP).

Conflicts of Interest: The authors declare no conflict of interest. The funding as stated in the Acknowledgement Section directly contributed to the equipment and the materials' preparation.

Nomenclature

x_1	First studied factor, temperature ($^{\circ}C$)
x_2	Second studied factor, holding time (min)
y_1	Ultimate tensile strength (MPa)
y_2	Elongation to failure (%)
y_3	Microhardness
HV	Vickers hardness
d.f.	Degrees of freedom
Prob. > F	Probability to get the stated F value
Cor. total	Total of all information corrected for the mean
Std. Dev.	Standard deviation
C.V. %	Percent coefficient of variation
PRESS	Predicted residual error sum of squares
R^2	Coefficient of determination
R^2_{adj}	Adjusted R^2
R^2_{pred}	Predicted R^2
Adeq. precision	Adequate precision

References

1. Rombach, G. *Integrated Assessment of Primary and Secondary Aluminium Production*; DMG Business Media, Ltd.: Surrey, UK, 1998.
2. International Aluminium Institute. *Global Aluminium Recycling: A Cornerstone of Sustainable Development*; International Aluminium Institute: London, UK, 2009.
3. Lajis, M.A.; Yusuf, N.K.; Ahmad, A. Life cycle assessment on the effects of parameter setting in direct recycling hot press forging of aluminum. *Mater. Sci. Forum.* **2018**, *923*, 143–148. [[CrossRef](#)]
4. Chawla, K.K. Metal matrix composites. In *Composite Materials*; Springer: New York, NY, USA, 2012.

5. Clyne, T.W.; Withers, P.J. *An introduction to Metal Matrix Composites*; Cambridge University Press: Cambridge, UK, 1995.
6. Sajjadi, S.A.; Parizi, M.T.; Ezatpour, H.R.; Sedghi, A. Fabrication of A356 composite reinforced with micro and nano Al₂O₃ particles by a developed compocasting method and study of its properties. *J. Alloys Compd.* **2012**, *511*, 226–231. [[CrossRef](#)]
7. Ibrahim, I.A.; Mohamed, F.A.; Lavernia, E.J. Particulate reinforced metal matrix composites—A review. *J. Mater. Sci.* **1991**, *26*, 1137–1156. [[CrossRef](#)]
8. Corrochano, J.; Cerecedo, C.; Valcárcel, V.; Lieblich, M.; Guitián, F. Whiskers of Al₂O₃ as reinforcement of a powder metallurgical 6061 aluminium matrix composite. *Mater. Lett.* **2008**, *62*, 103–105. [[CrossRef](#)]
9. Xia, Z.; Ellyin, F.; Meijer, G. Mechanical Behavior of Al₂O₃-Particle-Reinforced 6061 Aluminum Alloy Under Uniaxial And Multiaxial Cyclic Loading. *Compos. Sci. Technol.* **1997**, *3538*, 237–248. [[CrossRef](#)]
10. Mazahery, A.; Abdizadeh, H.; Baharvandi, H.R. Development of high-performance A356/nano-Al₂O₃ composites. *Mater. Sci. Eng. A* **2009**, *518*, 61–64. [[CrossRef](#)]
11. Akbulut, H.; Durman, M. Temperature dependent strength analysis of short fiber reinforced Al-Si metal matrix composites. *Mater. Sci. Eng. A* **1999**, *262*, 214–226. [[CrossRef](#)]
12. Groover, M.P. *Principles of Modern Manufacturing*, 4th ed.; John Wiley & Sons: Hoboken, NJ, USA, 2011.
13. Altan, T.; Ngaile, G.; Shen, G. *Cold and Hot Forging*; ASM international: Cleveland, OH, USA, 2005.
14. Yusuf, N.K.; Lajis, M.A.; Ahmad, A. Hot Press as a Sustainable Direct Recycling Technique of Aluminium: Mechanical Properties and Surface Integrity. *Materials* **2017**, *10*, 902. [[CrossRef](#)]
15. Yusuf, N.K. A New Approach of Direct Recycling Aluminium Alloy Chips (AA6061) In Hot Press Forging Process. Ph.D. Thesis, Universiti Tun Hussein Onn Malaysia, Parit Raja, Malaysia, 2013.
16. Semiatin, S.L. *ASM Handbook, Volume 14: Forming and Forging*; Materials Park: Cleveland, OH, USA, 1996.
17. Yusuf, N.K.; Lajis, M.A.; Daud, M.I.; Noh, M.Z. Effect of Operating Temperature on Direct Recycling Aluminium Chips (AA6061) in Hot Press Forging Process. *Appl. Mech. Mater.* **2013**, *315*, 728–732. [[CrossRef](#)]
18. Lajis, M.A.; Khamis, S.S.; Yusuf, N.K. Optimization of Hot Press Forging Parameters in Direct Recycling of Aluminium Chip (AA 6061). *Key Eng. Mater.* **2014**, *622–623*, 223–230. [[CrossRef](#)]
19. Ahmad, A.; Lajis, M.A.; Shamsudin, S.; Yusuf, N.K. Conjectured the behaviour of a recycled metal matrix composite (MMC-Al_R) developed through hot press forging by means of 3D FEM simulation. *Materials* **2018**, *11*, 958. [[CrossRef](#)] [[PubMed](#)]
20. Ahmad, A.; Lajis, M.A.; Yusuf, N.K.; Shamsudin, S.; Zhong, Z.W. Parametric optimisation of heat treated recycling aluminium (AA6061) by response surface methodology. *AIP Conf. Proc.* **2017**, *1885*. [[CrossRef](#)]
21. Khamis, S.S.; Lajis, M.A.; Albert, R.A.O. A Sustainable Direct Recycling of Aluminum Chip (AA6061) in Hot Press Forging Employing Response Surface Methodology. *Procedia CIRP* **2014**, *26*, 477–481. [[CrossRef](#)]
22. Durrant, G.; Scott, V.D. The effect of forging on the properties and microstructure of saffil fibre reinforced aluminum. *Compos. Sci. Technol.* **1993**, *49*, 153–164. [[CrossRef](#)]
23. Ahmad, A.; Lajis, M.A.; Yusuf, N.K. On the role of processing parameters in Producing recycled aluminum AA6061 based metal matrix composite (MMC-Al_R) prepared using hot press forging (HPF) process. *Materials* **2017**, *10*, 1098. [[CrossRef](#)]
24. Prabhu, B.; Suryanarayana, C.; An, L.; Vaidyanathan, R. Synthesis and characterization of high volume fraction Al–Al₂O₃ nanocomposite powders by high-energy milling. *Mater. Sci. Eng. A* **2006**, *425*, 192–200. [[CrossRef](#)]
25. Lajis, M.A.; Yusuf, N.K.; Noh, M.Z. Mechanical Properties and Surface Integrity of Direct Recycling Aluminium Chips (AA6061) by Hot Press Forging Process. In Proceedings of the 11th Global Conference on Sustainable Manufacturing, Berlin, Germany, 23–25 September 2013.
26. Lajis, M.A.; Yusuf, N.K.; Noh, M.Z.; Ibrahim, M. Effect of Chip Size on Direct Recycling of Aluminium Chips (AA6061) in the Hot Press Forging Process. *Int. Solid Waste Assoc.* **2013**, 120–125.
27. Ahmad, A.; Lajis, M.A.; Yusuf, N.K.; Wagiman, A. Hot Press Forging as The Direct Recycling Technique of Aluminium—A Review. *ARPN J. Eng. Appl. Sci.* **2016**, *11*, 2258–2265.
28. Lajis, M.A.; Ahmad, A.; Yusuf, N.K.; Azami, A.H.; Wagiman, A. Mechanical properties of recycled aluminium chip reinforced with alumina (Al₂O₃) particle: Mechanische Eigenschaften von mit Aluminiumoxid (Al₂O₃) verstärkten recycelten Aluminiumspänen. *Mater. Werkst.* **2017**, *48*, 306–310. [[CrossRef](#)]
29. Yusuf, N.K. Effects of Hot Press Forging Parameter and Life Cycle Assessment In Direct Recycling of AA6061 Aluminium. Ph.D. Thesis, Universiti Tun Hussein Onn Malaysia, Parit Raja, Malaysia, 2017.

30. Daneshpayeh, S.; Ghasemi, F.A.; Ghasemi, I.; Ayaz, M. Predicting of mechanical properties of PP/LLDPE/TiO₂ nano-composites by response surface methodology. *Compos. Part B Eng.* **2016**, *84*, 109–120. [[CrossRef](#)]
31. Myers, R.H.; Montgomery, D.C.; Anderson-Cook, C.M. *Response Surface Methodology: Process and Product Optimization Using Designed Experiments*; John Wiley & Sons: Hoboken, NJ, USA, 2009.
32. Montgomery, D.C. *Design and Analysis of Experiment*; John Wiley Sons: New York, NY, USA, 1997; p. 445.
33. Han, Y.-L.; Gao, J.; Yin, Y.-Y.; Jin, Z.-Y.; Xu, X.-M.; Chen, H.-Q. Extraction optimization by response surface methodology of mucilage polysaccharide from the peel of *Opuntia dillenii* haw. fruits and their physicochemical properties. *Carbohydr. Polym.* **2016**, *151*, 381–391. [[CrossRef](#)] [[PubMed](#)]
34. Montgomery, D.C. *Design and Analysis of Experiments*; John Wiley & Sons: Hoboken, NJ, USA, 2013.
35. Muhamad, M.H.; Abdullah, S.R.S.; Mohamad, A.B.; Rahman, R.A.; Kadhum, A.A.H. Application of response surface methodology (RSM) for optimisation of COD, NH₃-N and 2,4-DCP removal from recycled paper wastewater in a pilot-scale granular activated carbon sequencing batch biofilm reactor (GAC-SBBR). *J. Environ. Manag.* **2013**, *121*, 179–190. [[CrossRef](#)] [[PubMed](#)]
36. Triveni, R.; Shamala, T.R.; Rastogi, N.K. Optimised production and utilisation of exopolysaccharide from *Agrobacterium radiobacter*. *Process Biochem.* **2001**, *36*, 787–795. [[CrossRef](#)]
37. Salim, N.; Hashim, R.; Sulaiman, O.; Ibrahim, M.; Sato, M.; Hiziroglu, S. Optimum manufacturing parameters for compressed lumber from oil palm (*Elaeis guineensis*) trunks: Respond surface approach. *Compos. Part B Eng.* **2012**, *43*, 988–996. [[CrossRef](#)]
38. Derringer, G.; Suich, R. Simultaneous optimization of several response variables. *J. Qual. Technol.* **1980**, *12*, 214–219. [[CrossRef](#)]
39. Islam, M.A.; Alam, M.R.; Hannan, M.O. Multiresponse optimization based on statistical response surface methodology and desirability function for the production of particleboard. *Compos. Part B Eng.* **2012**, *43*, 861–868. [[CrossRef](#)]
40. Lazo-Vélez, M.A.; Avilés-González, J.; Serna-Saldivar, S.O.; Temblador-Pérez, M.C. Optimization of wheat sprouting for production of selenium enriched kernels using response surface methodology and desirability function. *LWT-Food Sci. Technol.* **2016**, *65*, 1080–1086. [[CrossRef](#)]
41. ASTM B328-96. *Standard Test Method for Density, Oil Content, and Interconnected Porosity of Sintered Metal Structural Parts and Oil-Impregnated Bearings*; ASTM International: West Conshohocken, PA, USA, 2003; Volume 96, pp. 1–4.
42. Joglekar, A.M.; May, A.T.; Graf, E.; Saguy, I. Product excellence through experimental design. In *Food Product and Development: From Concept to the Marketplace*; Springer Science & Business Media: Berlin, Germany, 1987; pp. 211–230.
43. Ahmad, A.L.; Wong, S.S.; Teng, T.T.; Zuhairi, A. Optimization of coagulation-flocculation process for pulp and paper mill effluent by response surface methodological analysis. *J. Hazard. Mater.* **2007**, *145*, 162–168. [[CrossRef](#)]
44. Rahimian, M.; Ehsani, N.; Parvin, N.; Baharvandi, H.R. The effect of sintering temperature and the amount of reinforcement on the properties of Al-Al₂O₃ composite. *Mater. Des.* **2009**, *30*, 3333–3337. [[CrossRef](#)]
45. Daoud, A. Wear performance of 2014 Al alloy reinforced with continuous carbon fibers manufactured by gas pressure infiltration. *Mater. Lett.* **2004**, *58*, 3206–3213. [[CrossRef](#)]

